Supplemental Materials: Table of Contents

Supplemental Materials

Participant Inclusion/Exclusion Criteria

Study inclusion criteria included a diagnosis of T2DM based on clinical report of a diagnosis of T2DM from a physician, confirmation of medication usage for DM (insulin, oral hypoglycemic agents or both) and verification of HbA1c levels either currently or at the time of diagnosis >6.5%, and/or OGTT >200 mg/dL. A diagnosis, particularly for those with eGFR <60 mL/min, of diabetic nephropathy based on nephrologist clinical assessment of patient medical history, degree of proteinuria (must be present at least at the microalbuminuria level – urinary ACR >30 mg/g), glycemic control, diabetic medication use, hypertension status, and rate of kidney decline (eGFR utilizing creatinine), all according to KDIGO guidelines.

Participants were excluded from the study if they weighed more than 350 pounds (equipment weight limit), had any infection or ulceration of either foot, severe foot deformity or amputation, or any serious medical co-morbidity -- dialysis treatment, heart failure requiring medications, or New York Heart Association class 3 or class 4 heart failure, coagulation disorders, anemia (Hgb < 10g/dL), uncontrolled proliferative diabetic retinopathy, joint replacement or musculoskeletal injury that precludes intense muscular contraction, within 1 year of enrollment, may be pregnant or breast feeding, current cancer treatment, and organ transplant requiring immunosuppressant therapy, or individuals who are participating in regular and/or structured exercise programs. Additionally, to specifically determine/ensure sedentary status, all prospective participants were defined according to the Sedentary Behavior Research Network criteria -- any waking behavior characterized by energy expenditure <1.5 metabolic equivalents, while not engaging in any moderate-to-vigorous physical activity (any activity >3 metabolic equivalents) during the day, on a day-to-day basis (**59**).

Physical Performance Test Sub-Item Descriptions

The PPT is a timed observational assessment of performance on nine daily physical activities that break down as follows-

(1) 5 consecutive sit-to-stand chair rises without arm assistance, (2) climbing a flight of stairs with 10 steps, (3) a 50-ft. walk test, (4) turning 360 degrees, (5) picking up a penny from the floor, (6) donning/doffing a jacket, (7) lifting a book onto an overhead shelf, (8) a Romberg standing balance assessment with eyes open, (9) and ability to ascend 4 flights of stairs [**55**]. Each item is scored from 0-4 based on the time taken to complete each task, with a maximum score of 36 (higher scores indicate better physical function/performance and less time taken to complete each task). Each task is performed twice with the average time used to score the task.

The mPPT possesses a test-retest reliability of .964, while individual sub-items have reliability ranging from .51-.99, and Cronbach alpha of .785 [**S1,S2,S3**].

During physical functional testing, individuals were asked to rate the degree of difficulty of the physical task on a 10-point visual analogue scale, soon after completing the specific activity. Similarly, all participants were consistently monitored and prompted to report any symptoms of fatigue, chest pain, palpitations, or shortness of breath during functional testing.

Muscle Performance Assessment

The tested leg was weighted to correct for the effects of gravity on the torque measured, according to the specifications of the Biodex Manual. Range of motion was set for each movement to obtain ~110 degrees of hip flexion (from ~5° of hip extension), ~90 degrees of knee flexion (from terminal extension). Participants were seated upright for knee extensor muscle performance testing, and placed in supine with trunk slightly bolstered, for hip muscle testing. Hip and knee joint centers were aligned to the axis of dynamometer rotation. Prior to each test, participants were familiarized with procedures by performing 3-5 submaximal contractions. The isokinetic tests for each muscle group included 5 maximal concentric contractions at

movement speeds of 30°/sec and 120°/sec, with the highest 3 repetitions averaged to determine peak torque (ft-lbs.). Isometric tests consisted of 4 maximal contractions held for 5 seconds each. Isometric force production was assessed at 60^0 hip flexion, 60^0 knee flexion [**S4,S5**]. Maximal concentric torque production and isometric torque repetitions were separated by 5 seconds rest. Power was determined by the time-averaged integrated area under the curve at the constant velocity of movement in the available range of motion during the isokinetic testing. At each of the repetitions, seconds to peak torque, and power was assessed and averaged.
Fatigue Protocol - participants performed 50 maximal repetitions at 90^0/sec, with 2 second rest period between repetitions. Torque production was assessed for each repetition, and work was calculated across the first, second, and third portion of the fatigue set, and totaled for an index of fatigue resistance [**22,4**].

Fasting/medication/OGTT
Participants refrained from eating for 10 hours prior to administration of the 3-hour oral glucose tolerance test. All diabetes medications (except insulin) were stopped 2 days before study admission to decrease residual drug effects on the metabolic measurements (long-acting GLP-1 agonist and thiazolidinediones were stopped 7 days before admission). Subcutaneous insulin was stopped after the final dose on the day prior to admission. Participants' fasting plasma glucose was assessed 10 minutes prior to administration of a 75g glucose drink and again at the time of drink ingestion, 10, 20, 30 minutes, and then every half hour until 3 hours post-ingestion. HOMA-IR is calculated as -- [(fasting glucose (mg/dL)] x [fasting insulin (μU/mL)]/405 [**24**].

Muscle Biopsy Procedure
2 weeks after skeletal muscle performance and functional assessments, participants returned for metabolic and tissue-based assessments. Participants were positioned supine in a hospital bed with the thigh of their dominant leg exposed (opposite to the leg tested for muscle performance). Participants were then asked to contract the thigh so as to visualize the vastus lateralis (anterior to fascia lata, approximately $1/3^{rd}$ of the distance from patella to great trochanter). The area was prepped and cleaned with iodine, and draped. The skin was anesthetized with 2% lidocaine solution injected into the dermis and allowed to take effect over a 3-minute period. A 1-2 cm incision was made through the skin and subcutaneous tissue, and a 5 mm Bergstrom needle was introduced with vacuum suction into the vastus lateralis. 2 passes of the biopsy needle were performed for each participant obtaining ~250-350 mg of skeletal muscle tissue as previously described [**S6**]. ~50-75 mg of the sample was immediately snap-frozen in liquid nitrogen and stored at -80°C until further analysis (mtDNA copy number, qPCR, enzyme testing, RNA-sequencing).

Mitochondrial Functional Analysis Approach and Buffer compositions
A 10-mg sample of the vastus lateralis muscle biopsy was trimmed of surrounding epithelial and fat tissue and immediately placed into ice-cold relaxing buffer (buffer and media composition listed below). Trimmed fiber bundles were teased apart, on ice, and permeabilized in freshly prepared saponin permeabilization solution (composition below) on a rocker at 4°C for 20 minutes. After equilibration in respirometry media (15 minutes), samples were blot dried, weighed, and split into two 3-mg samples for respiratory assessment.
Oxygen flux was initially measured by adding malate (.5 mM), followed by glutamate (10 mM), and pyruvate (5 mM), in the absence of ADP (***State 2-C1, i.e. LEAK state respiration***). State 3 respiration using complex 1 (C1) substrates (state 3-C1) was then achieved by the addition of ADP (5 mM). This was followed by the addition of succinate (10 mM) to reach state 3 respiration through both C1 and complex 2 (C2) (***State 3-C1+C2***). As a quality control measure, cytochrome c (10 μM) was then added to the chamber (any increase is oxygen flux with cytochrome c administration would indicate damage to the normally impermeable outer mitochondrial membrane during preparation). Oxygen flux changes that did not exceed 15% upon cytochrome c

administration, were deemed evidence of non-damaging permeabilization as described previously [**S7**]. Next, carbonylcyanide-4-(trifluoromethoxy)-phenyl-hydrazone (FCCP) was titrated (3x, .5uM) to assess maximal respiratory flux through the electron transfer system in the uncoupled state (***ETS capacity – state E***) [**S8**]. Additional flux-control ratios were calculated to gain further insights into mitochondrial coupling efficiency and included -- oxidative phosphorylation system control ratio (***P/E; phosphorylation system deficits***), respiratory-control ratio (***RCR – P/L; coupling efficiency of mitochondria***), phosphorylation control ratio (***L/P; indicative of increased dyscoupling***), oxidative phosphorylation coupling efficiency ratio (***L-P)/P), ETS coupling efficiency ((E-L)/E; ratios closer to 1 indicate more efficient mitochondrial coupling***)

Relaxing Buffer = 50 mM K+-MES, 20 mM taurine, 0.5 mM dithiothreitol, 6.56 mM MgCl2, 5.77 mM ATP, 15 mM phosphocreatine, 20 mM imidazole, pH 7.1, adjusted with 5 N KOH at 0 °C, 10 mM Ca–EGTA buffer (2.77 mM CaK2EGTA + 7.23 mM K2EGTA; 0.1 μM free calcium)
Saponin permeabilization solution = .003% saponin – weight/volume in relaxing buffer
Respirometry media = 110 mM sucrose, 60 mM K+-lactobionate, 0.5 mM EGTA, 3 mM MgCl2, 20 mM taurine, 10 mM KH2PO4, 20 mM HEPES adjusted to pH 7.1 with KOH at 37 °C; and 1 g/l BSA essentially fatty acid free
For respiration assessment: per oroborus chamber - 2.1 mL of respirometry media supplemented with 2.1 uL of 10μM blebbistatin and 6.3 mg creatine)
FCCP = FCCP is a protonophore that collapses the electrochemical proton potential across the inner mitochondrial membrane, thereby removing the electrochemical backpressure on the proton pumps and represents maximal respiration in the uncoupled state **[S8**].

Respirometry Chamber Setup
Blot-dried samples were split into two 3-mg samples, and placed into the respirometry chamber (one 3-mg sample per chamber) (OROBORUS). Chamber parameters were set to 37°C internal temperature, with a stirrer speed of 750 rpm (12.5 Hz), with an oxygen flux data collection interval of 2 seconds, and filled with respirometry media (per chamber - 2.1 mL of respirometry media supplemented with 2.1 uL of 10μM blebbistatin and 6.3 mg creatine).

Flux Control Ratio Descriptions
Oxidative Phosphorylation System Control Ratio (P/E): Ratio of max oxidative phosphorylation (P) to max electron transfer capacity (E). Assessed to analyze for phosphorylation system deficits as lower ratios indicate phosphorylation deficit within mitochondria.
Respiratory Control Ratio or RCR (P/L): Ratio of max oxidative phosphorylation (P) to LEAK respiration (L). Provides insight into the coupling efficiency of mitochondria, with higher values indicating improved coupling.
Phosphorylation Control Ratio (L/P): Ratio of LEAK respiration (L) to max oxidative phosphorylation (P). Higher values are indicative of increased dyscoupling.
Oxidative Phosphorylation Coupling Efficiency Ratio (L-P)/P: The ratio of max oxidative phosphorylation (P) subtracted from LEAK respiration, to max oxidative phosphorylation (P). Lower or more negative values indicate more efficient coupling of the ETC to ATP production
ETS Coupling Efficiency (E-L)/E: The ratio of LEAK respiration (L) subtracted from maximal electron transfer capacity (E), to maximal electron transfer capacity (E). Ratios closer to 1 indicate more efficient mitochondrial coupling of ATP production, as this would indicate small contribution of LEAK respiration to maximal transfer capacity.

Mitochondrial DNA Copy Number
From the flash frozen sample, a 20 mg portion was used for DNA extraction using a QIAgen DNeasy Blood and Tissue Kit (QIAGEN, Valencia, CA) according to the manufacturer's instructions. Muscle samples were lysed with 100 uL of the supplied buffer (Buffer ATL) for 50-90 minutes in the presence of proteinase K (2.5 mg/mL)

in a 70°C water bath. The lysis was completed by adding 200 uL of buffer AL and incubating at 70°C for 10 minutes. The entire mixture was then applied to a provided spin column, centrifuged at 8000 rpm for 1 min., and washed twice with 500 uL supplied wash buffer (Buffer AW), and DNA eluted three times with elution buffer (buffer AE). Following DNA isolation, precise quantitation of DNA was obtained via nanodrop. DNA concentrations ranged from 20-45 ng/uL per sample.
mtDNA copy number was assessed with oligonucleotide primers for mtDNA-encoded 12s ribosomal RNA and nucleus-encoded β2 microglobulin:
Nuclear genome B2-microglobulin gene (forward 5'- TGCTGTCTCCATGTTTGATGTATCT-3', reverse 5'-TCTCTGCTCCCCACCTCTAAGT-3')]
Mitochondrial genome 12s Ribosomal RNA [mt806 (forward 5'-CCACGGGAAACAGCAGTGATT-3', mt929 (reverse 5'-CTATTGACTTGGGTTAATCGTGTGA-3')
For RT-PCR, DNA was diluted to 2 ng/uL in DEPC water with both forward and reverse primers, and added to 10 uL of 2x PCR SYBR Green mastermix and 9.2 uL of DEPC water (total volume per reaction – 20 uL) per well in a 96-well plate and covered with optical adhesive. Sample PCRs were run in triplicate per gene probe on an Applied Biosystems ABI 7300 real-time PCR system. mtDNA and nDNA Ct values were averaged from the triplicate. To determine mtDNA content relative to nuclear DNA, the ΔCt method was used -- ΔCt = (*n*DNA Ct – *mt*DNA Ct), where relative mitochondrial DNA content = $2x2^{\Delta Ct}$ [**26**].

Mitochondrial Enzymatic Testing
Average size of the muscle biopsy was ~100-150 mg of tissue. 20 mg of tissue was taken for respirometry assessment, 20 mg was utilized for mtDNA copy number analyses, 50-75 mg was reserved for next-gen sequencing (~90-115 mg accounted for). Thus, given the requirement of 50 mg of tissue for enzymatic functional analyses, not every participant had enough tissue for these measures. We performed these tests on individuals when the remaining muscle sample permitted – resulting in the 13 participants shown here. In this respect, participant selection was random, and spread between CKD stages.

NADH dehydrogenase: 300 uL of the frozen muscle homogenate supernatants were thawed at 2-4^{0}C, centrifuged (14000g) and supernatant collected for complex 1 enzymatic activity as previously described [**27,S10**]. Complex 1 oxidizes NADH, with resulting electrons capable of reducing artificial substrates, such as decylubiquinone, that deliver these electrons to 2,6-dichloroindophenol (DCIP). The reduction of DCIP is then tracked spectrophotometrically (600 nm wavelength). Thus, complex 1 enzyme activity was assessed spectrophotometrically at 600 nm, with incubation volume of 1 mL, supplemented with 25 mmol/L potassium phosphate, 3.5 g/L BSA, 60 umol/L DCIP, 70 umol/L decylubiquinone, 1 umol/L antimycin-A, and .2 mmol/L NADH, pH 7.8. The muscle homogenate was mixed with the reaction solution (1 mL) at 37^{0}C, and measured the absorbance at 30-second intervals for 10 minutes. Complex 1 activity was expressed as umol/min/gram tissue.

Citrate Synthase Activity: Serves as a measure of mitochondrial density/abundance. Each sample was run in duplicate as previously described [**27**]. CS was determined spectrophotometrically at 30 deg C by measuring decreased absorbance of Acetyl CoA at 232 nM, due to the hydrolysis of the thioester in the formation of CoA-SH with CS activity. Muscle samples were homogenated in .5mL of medium consisting of 50 mM Tis HCL (pH 7.4) and .15M KCL and aliquoted and stored at -80 deg C for subsequent enzymatic analysis.
In a water bath, maintained at 30 deg Celsius to increase reaction kinetics, samples were prepared by adding 1 mL of 100 mM Tris (pH 8.1), used as a buffer, 3.4 uL of .17 mM Oxaloacetic Acid, and 10 uL of .2M Acetyl CoA. The samples were poured into a quartz cuvette and inserted into a UNICO spectrophotometer maintained at 30 deg c. Readings were taken at 232 nM, the ideal wavelength for Acetyl CoA thioester absorption at 1-minute intervals for 10 minutes. The absorbance values were then plotted against time and the rate of absorbance decay determined and expressed per minute per gram tissue as described previously [**S9**].

SDH Enzymatic Activity (Complex 2): 10 uL of the 1:10 muscle homogenate was added to 100 uL of freshly made assay reagent. Briefly, fresh assay reagent consists of .5mL of 1M Imidazole HCL (pH 7.4) for a reaction concentration of 50mM, 1 mL of 1M succinate for a final concentration of 100 mM, .2 mLs of 500mM K_3FeCN_6 for an assay concentration of 10 mM, and finally, .2 mLs of 1% BSA. Once added, homogenate/assay mixture is incubated at room temperature for 60 minutes. Subsequently, 10 uL of 1N NaOH is added and heated at 60^0C for 20-minutes, followed by addition of 1mL fumarate indicator reagent (50mM 2-amino2 methyl propaneidol+200uM NAD+10mMglutamate+50ug/mL pig heart fumarase+2ug/mL GOT). Samples were read at 340 nM in a UNICO spectrophotometer, using disposable semi-micro cuvettes after the final reaction was complete (15-30 minutes) and expressed as umoles/min/gram [**27,S10**].

COX Enzyme Testing (Complex 4): Enzymatic analysis of complex 4 of the ETC is based on the principle that absorption of cytochrome C at 550 nm changes with its oxidation state. Its oxidation by cytochrome oxidase (complex 4) is a measure of COX activity. 5 uL of muscle homogenate is added to a cuvette containing .95 mL of .01M phosphate buffer (pH 7), and 50 uL of 1% reduced cytochrome C, and measured with a UNICO spectrophotometer at wavelength of 550 nm at 15, 30, 45, and 60 minutes. COX activity is expressed as described in citrate synthase above [**27**].

Transcriptome/RNA-seq

Tissue and Library Preparation (RNA isolation)-

Snap frozen tissue (per participant), was ground into a fine powder in a liquid-nitrogen cooled mortar and pestle and emptied into a vial containing 1mL of Trizol reagent (Invitrogen # 15596026) supplemented with 20 mg/mL glycogen and incubated for 10 minutes, and precipitated with chloroform, centrifuged at 13200 rpm (16000g) for 15 minutes, and the aqueous layer was transferred, precipitated with isopropanol and centrifuged at 13200 rpm (1600g) for 10 minutes. Finally, the pellet was re-suspended in 75% ethanol and centrifuged at 11000 rpm for 5 minutes and allowed to air dry for 15 minutes and re-suspended in DEPC water. Concentration and quality of mRNA were measured using a nanodrop spectrophotometer. Total RNA was subjected to clean-up using RNeasy kit (Qiagen).

The resulting cDNA ends were rendered blunt, an A base was added to the 3' ends, and Illumina sequencing adapters were ligated to the ends. The ligated fragments were then amplified for 12 cycles using primers that incorporated unique index tags, and the resulting fragments were sequenced on an Illumina HiSeq 2500 system using single reads that extended 50 bases and targeted 30M reads per sample as previously described [**S11**].

Sequencing-

RNA-seq reads were aligned to the Ensembl top-level assembly with STAR version 2.0.4b [**S12]**. Sequencing performance was assessed for total number of aligned reads, total number of uniquely aligned reads, genes and transcripts detected, ribosomal fraction known junction saturation and read distribution over known gene models with RSeQC version 2.3 [**S13**].

All gene-level and transcript counts were then imported into the R/Bioconductor package EdgeR and TMM normalization size factors were calculated to adjust for samples for differences in library size [**S14,S11**]. The TMM size factors and the matrix of counts were then imported into R/Bioconductor package Limma and weighted likelihoods based on the observed mean-variance relationship of every gene/transcript and sample were then calculated for all samples with the "voomWithQualityWeights" function. Performance of the samples was assessed with a spearman correlation matrix and multi-dimensional scaling plots. Gene/transcript performance was also assessed with plots of residual standard deviation of every gene to their average log-count with a robustly fitted trend line of the residuals. The muscle samples contained 44,000–66,000 transcripts, with ~5,000-8,000 genes detected, with the ribosomal fraction constituting <5% across all samples.

To determine the similarity between expression profiles, we used Pearson correlation plots. The correlation values indicate closely similar expression values for transcripts between biological samples. Gene counts were derived from the number of uniquely aligned unambiguous reads by Subread:featureCount version 1.4.5 [**28**]. Transcript counts were produced by Sailfish version 0.6.3. Generalized linear models were then created to test for gene/transcript level differential expression.

Assessment of Differential Gene Expression-
Differentially expressed genes in the stage 1&2 CKD group, stage 3 CKD group, and stage 4&5 CKD were filtered based on the highest fold change and significant *p*-values and the genes were annotated using Ensembl, leading to the identification of genes that were significantly altered between stages of disease.

Ribosomal Transcript allocation -
Ribosomal features as well as any feature not expressed in at least the smallest condition size minus one sample were excluded from further analysis and TMM size factors were recalculated to created effective TMM size factors.

Determination of significant GO terms and KEGG pathways-
The biological interpretation of the large set of features found in the Limma results were then elucidated for global transcriptomic changes in known Gene Ontology (GO) and KEGG terms with the R/Bioconductor packages GAGE and Pathview [**S15,S16**]. GO or KEGG terms were deemed significant based on changes in observed log 2-fold-changes for the genes within that term, with an adjusted statistical significance of FDR < 0.05. GAGE measures for perturbations in GO or KEGG terms based on changes in observed log 2-fold-changes for the genes within that term versus the background log 2-fold-changes observed across features not contained in the respective term as reported by Limma. For GO terms with an adjusted statistical significance of FDR <= 0.05, heatmaps were automatically generated for each respective term to show how genes co-vary or co-express across the term in relation to a given biological process or molecular function. In the case of KEGG curated signaling and metabolism pathways, Pathview was used to generate annotated pathway maps of any perturbed pathway with an unadjusted statistical significance of p-value <= 0.05.

Gene Set Enrichment Analyses and Leading Edge Assessment-
We rank ordered all transcripts from next-gen sequencing according to the correlation of their expression profiles with renal function (eGFR) from top positively correlated to bottom negatively correlated genes. Gene set enrichment analysis (GSEA) and leading edge analysis were then performed using the GSEA v2.2.4 (Broad Institute, Cambridge, MA). Gene sets carried forward for enrichment map construction and leading edge analyses were filtered based on an FDR Q<.05, and significance P-value <.05 (against the null-distribution ranked list obtained from 1000-permutation distribution of randomized rank order lists). Thus, we generated two gene sets from each assigned biological comparison for the top positively correlated genes and bottom negatively correlated genes with renal function. For enrichment map construction, network node thresholds were set at FDR Q = .01, and gene sets of interest were further selected based on the highest normalized enrichment score (NES) for final leading edge analysis as previously described (**S17**).

Supplemental Results

Mitochondrial Function/Coupling Efficiency

(1) No samples exhibited an increase in respiration exceeding 15% with cytochrome-c administration, indicating no mechanical damage was inflicted to the outer mitochondrial membrane in preparation.

(2) Power analysis of State3-C1, controlling for CS-activity, reveals that 10 participants would be needed per stage for this measure to reflect the unadjusted (not controlling for CS) respirometry measure differences for State3-C1.

Mitochondrial Enzyme Activity (13-participant subset)

(1) Power analysis of mt-DNA copy number (Fig.2A), reveals an effect size of f= .498, partial eta square of .199. This dictates that a total sample size of 45 participants (n=15 per CKD stage group) would be required to reach statistical significance (alpha <.05, power = 80%).
(2) Power analysis of CS-enzyme activity (Fig.2B), reveals an effect size of f= .497, partial eta square of .198. This dictates that a total sample size of 45 participants (n=15 per CKD stage group) would be required to reach statistical significance (alpha <.05, power = 80%).
(3) Power analysis of C2-enzyme activity (Fig.2C), reveals an effect size of f= .789, partial eta square of .384. This dictates that a total sample size of 21 participants (n=7 per CKD stage group) would be required to reach statistical significance (alpha <.05, power = 80%).
(4) Power analysis of C1-enzyme activity (Fig.2E), reveals an effect size of f= .79, partial eta square of .385. This dictates that a total sample size of 21 participants (n=7 per CKD stage group) would be required to reach statistical significance (alpha <.05, power = 80%).

Skeletal muscle neuromuscular performance:

	CKD Stage 1&2	CKD Stage 3	CKD Stage 4&5	P-Value
Seconds to peak Torque (Knee Ext. 120/sec)	.33 (.054)	.29 (.132)	.27 (.12)	.7 (ns)

Supplemental Tables

Table S1

Stage 3 vs. Stage 1&2 Significant GO and KEGG terms: selected genes	
Lipid Localization	
TSPO (-1.4x)	Promotes transport of cholesterol across mitochondrial membranes and may play a role in lipid metabolism. TSPO plays a central role in regulation of mitochondrial function modulating the crosstalk between inner membrane anion channel (IMAC) and permeability transition pore. In response to oxidative stress, and impaired antioxidant systems, TSPO is downregulated to prevent excessive superoxie anion ef□ux from the mitochondrial matrix and as an attempt to ensure the permeability transition pore is not enlarged (**S18**)
ADIPOQ (-7.4x)	Encodes adiponectin -- involved in the control of fat metabolism and insulin sensitivity,with anti-in□ammatory activities. Stimulates AMPK phosphorylation and activation in skeletal muscle, enhancing glucose utilization and fatty-acid combustion. Antagonizes TNF-alpha by negatively regulating its expression in and also by counteracting its effects. Inhibits NF-kappa-B signaling through a cAMP-dependent pathway. Muscle with reduced ADIPOQ shows increased oxidative stress, in□ammation. Restoration of adiponectin alleviates oxidative stress and in□ammation in skeletal muscle (**S19**)
LEP (-4.8X)	Leptin stimulates fatty acid oxidation in muscle via aAMPK, resulting in decreased IMAT accrual and suppresses lipotoxicity (**S20**)
STARD4 (-2.55x)	Plays a role in lipid metabolism (**S19**)
LDLR (-2.5x)	LDL-receptor -- de□iency leads to elevated LDL levels and myocellular adipose accumulation (**S21**)
ABCD2 (-2.3x)	Gene encoding peroxisomal import of fatty acids into mitochondria (**S22**)
PPARG (-1.4x)	Gene that stimulates adiponectin production from muscle (mirrors the reduced adipoq expression). Also plays role in mitochondrial biogenesis (**S20**)
Mitochondrial Organization	
MRPL12 (-2.4x)	Encodes mitochondrial ribosome, for mitochondrially encoded protein transcription. Loss of mitochondrial ribosomes would impair transcription of key mitochondrial-encoded proteins (**S23**)
SLC25A33 (-1.3x)	Encodes a mitochondrial transporter that participates in mt genome maintenance, and regulation of mitochondrial membrane potential and mitochondrial respiration. It also controls the ratio of mitochondria-to-nuclear encoded components of the ETC, resulting in control of mitochondrial ROS. With IGF-1 stimulation, it can regulate cell growth and proliferation by controlling mitochondrial DNA replciation and transcription (**47**)
TMEM70 (-2.4x)	Encodes a protein that plays a role in biogenesis of mitochondrial ATP synthase. Impaired expression can result in reduced oxidative phosphorylation via inadequate ATP-synthase (**S38**)
RRM2B (-1.8x)	A nuclear-encoded mitochondrial maintenance gene, and repair of damaged mitochondrial DNA (**45**)
DNA2 (-1.8x)	Encoded protein is a conserved helicase/nuclease involved in the maintenance of mitochondrial and nuclear DNA stability (**46**)
CTTN (-1.6x)	Encodes cortactin protein, which has been postulated, though still debated, to play a role in mitochondrial □sion. Downregulation may impede mitochondrial quality control mechanisms, speci□ally attenuating mitochondrial division
SLC35F6 (-1.6x)	SLC35F6 stimulates mitochondrial membrane potential by interacting with ATP transporter ANT2 embedded in the mitochondrial inner membrane to transport ATP out to the cytosol while importing ADP into the mitochondrial matrix. Mitochondrial biogenesis requires maintenance of this mitochondrial membrane potential for importing nuclear-encoded proteins involved in oxphos, mtDNA replication and transcription (**S24**)
CSNK2A2 (-1.44x)	CSNK2 phosphorylates TOMM receptor complex. TOMM is responsible for recognition and translocation of synthesized mitochondrial precursor proteins, and its phosphorylation is mandatory for TOMM biogenesis and proper mitochondrial protein import. Loss of TOMM phosphorylation can result in impaired protein subunit import into mitochondria (**S25**)
GRPEL2 (-1.52x)	Encodes an essential component of the "presequence translocase-associated motor" complex (PAM), that regulates protein import into the mitochondrial matrix. It also binds to several essential regulators of mitochondrial function. It also interacts with longevity-regulating mitochondrial Hsp70, and is also linked to mitochondrial function. It stimulates Hsp70, and plays a role in mitochondrial unfolding response (**S26**)
Oxidative phosphorylation	
NDUFAB1 (-1.94x)	Nuclear-encoded subunit of complex 1, functions in the transfer of electrons from NADH to chain. Reduces in expression with age, potentially connected to complex-1 respiratory de□iencies (**S27**)
PINK1 (-1.4X)	Encodes Pink1 -- part of the pink/parkin2 mitophagy pathway. Pink1 must accumulate on outer membrane of defective mitochondria where it activates parkin2, which then recruits autophagy receptors (i.e. p62) that facilitates docking to the autophagasome for degradation. Lack of pink1 can lead to impaired mitophagy, through disruption in Parkin localization to damaged mitochondria. Pink1 also controls mitochondrial □sion, and if □sion is interfered with, this leads to increased oxidized proteins and decreased mitochondrial respiration (**50**)
SOD2 (-1.63x)	Encodes superoxide dismutase 2, anti-oxidant that scavenges superoxide radical ROS products. If downregulated, could result in ine□ient ROS handling. Reducing SOD2 leads to fragmentation of mitochondria.
BCL2L1 (-1.5x)	BCL2L1 proteins belong to BCL2 family, located in the outer mitochondrial membrane and regulate mitochondrial membrane VDAC opening, which regulates mitochondrial membrane potential, and thus controls the production of ROS and release of cytochrome C -- inducers of cell apoptosis. Loss of BCL2L1 promotes increased VDAC opening – creating a permeation pathway for metabolites and mobile ions between the cytosol and mitochondria. VDACs are also involved in cell death by interacting with apoptotic proteins and releasing apoptotic metabolites to the cytosol (**S28**)
BAG4 (-1.4x)	Encodes mitochondrial-expressed stress protein Bag-4 that is anti-apoptotic. It is a negative regulator of parkin translocation following mitochondrial damage. Parkin gets recruited to Pink1 sites on mitochondria to degrade them (**50**)
STAT2 (-1.3x)	Required for DRP-1 mediated mitochondrial □sion, resulting in altered mitochondrial morphology. Reduced STAT2 results in altered JAK-STAT pathway signaling, and reduced mitochondrial □sion (**S29**)
NCF2 (-1.8x)	Protects against cell apoptosis via bene□ial p53-stimulated ROS production. If downregulated, results in increased cell apoptosis

Table S1. Table of significantly differentially expressed genes from Figure 1B (genes down or upregulated in middle-stage CKD vs. early stage 1&2), their relative fold change, and their basic function listed to the right.

Table S2

Stage 4&5 vs. Stage 1&2 Significant GO and KEGG terms: selected genes	
Oxidative Phosphorylation	
SPATA18 (+1.5x)	Encodes a p53-induced protein that induces lysosomal eliminiation of oxidized mitochondrial proteins, contributing to mitochondrial quality control. Responsible for repairing or degrading unhealthy mitochondria in response to mitochondrial damage. Involved in vacuolar lysosome degradation of damaged mitochondria.
PINK1 (-1.34x)	Encodes Pink -- part of the pink/parkin2 mitophagy pathway, whereby pink1 must accumulate on the outer membrane of defective mitochondria where it activates parkin2, which then recruits autophagy receptors like p62 causing them to be shuttled to the autophagasome for degradation. Lack of pink1 can lead to impaired mitophagy (**50**)
BCL2 (-1.4x)	Encodes BCL2 autophagy regulatory protein -- autophagasome formation requires the interaction of BCL2 and BECN1 (Beclin-1) protein, with Beclin-1 dissociation from BCL2 activating autophagasome formation and autophagy of deficient mitochondria (**S30**)
BECN1 (-1.3x)	Encodes Beclin-1, part of mitochondrial autophagy pathway. Forms crucial component of phagaphore which targets and removes defective mitochondria. Downregulation leads to impaired mitophagy and poor mitochondrial turnover (**S30**)
MSTO1 (+1.6x)	Encodes the MSTO1 Cytoplasmic protein that interacts with and is required for, mitochondrial fusion of damaged mitochondria (**S31**)
TP63 (+1.61x)	Encodes a member of the p53 family of transcription factors - p63. p63 regulates REDD1 gene transcription, which stimulates ROS production/increase. Thus, increased p63 increases ROS via REDD1 (**S32)**
TIGAR (-1.72x)	Encodes TIGAR - a p53 target that protects against oxidative stress in muscle cells by inhibiting glycolysis and decreasing ROS levels. If reduced, results in increased ROS production, and enhanced sensitivity to stress-related apoptosis (**S33**)
TIMM17A (-1.23x)	Encodes an essential component of TIM23 that is responsible for protein import into the mitochondria. TIMM17A is reduced under stress conditions -- resulting in the impaired biogenesis of mitochondrial proteins that depend on TIM23 and triggers stress-induced signaling pathways related to the mitochondrial unfolded protein response (mtUPR) (**S34**)
Electron Transport Chain	
GPD2 (+1.8x)	Encodes a respiratory chain dehydrogenase that transfers electrons to COQ carrier and can often promote reverse electron flow back to complex 1 or complex 2, and has been shown to a major site of electron leak and ROS production (**S35**)
MTND3 (-1.42X)	Encodes core subunit 3 of complex 1 -- NADH dehydrogenase
MT-ND6 (-1.4x)	Encodes subunit 6 (nqo6) of complex 1 -- NADH dehydrogenase
NDUFAF2 (-1.3x)	Encodes complex 1 assembly factor
MT-ATP6 (-1.46x)	Encodes subunit 6 of complex 5-- ATP synthase
MT-ATP8 (-1.4x)	Encodes subunit 8 of complex 5 -- ATP synthase
ATP5MC1 (-1.3x)	Encodes subunit c of complex 5 proton channel
ATP5MC3 (-1.3x)	Encodes subunit c of complex 5
MT-CYB (-1.4x)	Encodes subunit 3 of complex 3 – Coenzyme Q (CoQ)
COX5A (-1.3x)	Encodes subunit 4 of complex 4 -- Cytochrome C Oxidase (COX)
MT-CO2 (-1.35x)	Encodes subunit 2, of complex 4 – Cytochrome C Oxidase (COX): subunit 2 transfers electrons to the core of the complex
COX6A2 (-1.3x)	Encodes subunit 6a2 of complex 4 – Cytochrome C Oxidase (COX): subunit 6a2 regulates assembly of cytochrome c oxidase
MT-CO3 (-1.31x)	Encodes subunit 3 of complex 4 – Cytochrome C Oxidase (COX): subunit 3 serves as the core of the complex
COX7A2 (-1.3x)	Encodes subunit 7a-L of complex 4 – Cytochrome C Oxidase (COX)
SURF1 (-1.3x)	Encodes a 30 kDa transmembrane protein localized in the inner mitochondrial membrane. SURF1 promotes the association of COX2 with the COX assembly intermediate composed of COX1, COX4 and COX5A. Reduced expression may hinder construction of COX complex (complex 4) of the ETC
Muscle structural Integrity	
SH3BGRL3 (-1.4X)	Plays a role in sarcomere assembly by encoding Enah protein -- localizes to the z-line to provide construction assistance for sarcomere assembly. Lack of SH3BGRL3 gene expression results in insufficent Enah protein recruitment to z-disc for sarcomere construction (**S36)**
DCN (-2.1x)	Encodes Decorin protein that counters the action of myostatin, and TGF-beta-mediated fibrosis. Also promotes mitochondrial biogenesis via PGC-1a activation. (**S37**)
MDM2 (+1.7)	Encodes a member of E3 ubiquitin ligase, activates FOXO3 atrophy pathways. MDM2 gets imported into mitochondria to control respiration and mitochondrial dynamics, and represses transcription of NADH-dehydrogenase6 (MT-ND6) which inhibits complex 1 activity and enhances mitochondrial ROS production (**37**)

Table S2 Table of significantly differentially expressed genes from Figure 1C (genes down or upregulated in late-stage CKD vs. early stage 1&2), their relative fold change, and their basic function listed to the right.

Table S3

	Stage 1&2 (60+ mL/min)	Stage 3 (30-59 mL/min)	Stage 4&5 (<29 mL/min)	P-value
Phosphorylation Control Ratio - PCR (L/P), (SD)	**.047 (.007)**	**.078 (.015)**	**.15 (.08)**	**(p=.001) *Stage 1&2 vs. Stage 3 ^Stage 1&2 vs. Stage 4&5**
Oxidative Phosphorylation Coupling Ef[illegible]ciency Ratio OPC ((L/P)/P), (SD)	**-.95 (.007)**	**-.92 (.015)**	**-.84(.08)**	**(p=.001) ^Stage 1&2 vs. Stage 4&5 #Stage 3 vs. Stage 4&5**
ETS Coupling Ef[illegible]ciency ((E-L)/E), (SD)	**.963 (.007)**	**.936 (.01)**	**.908 (.026)**	**(p<.001) *Stage 1&2 vs. Stage 3 ^Stage 1&2 vs. Stage 4&5 #Stage 3 vs. Stage 4&5**

Mitochondrial Respiratory Ratios. CKD-stage groups were compared in mitochondrial flux control ratios using 1-way ANOVA. Letters denote the following – P = max oxidative phosphorylation capacity (State 3-C1+C2), E = ETS capacity, L = state2-C1 (LEAK). Values listed are mean and standard deviation in (). ETS Coupling Efficiency – values closer to 1 are indicative of better coupling. The following symbols represent post-hoc pairwise comparisons in the event of significant F-test - *(between Stage 1&2 and Stage 3), ^(between stage 1&2 and Stage 4&5), #(Between stage 3 and Stage 4&5)

Table S4

	BMI	Whole-body Fat (%)	Trunk Fat (%)	Mito Max Oxphos	Mito Max ETS	Mito C1 Resp.	Mito Max Oxphos (normalized to CS)
BMI	r=1 p=----	r=.62 p=.001	r=.70 p<.001	r=-.27 p=.181	r=-.194 p=.354	r=-.331 p=.107	r=.195 p=.544
Whole-body Fat (%)	r=1 p=----	r=.948 p<.001	r=-.184 p=.39	r=-.082 p=.705	r=-.287 p=.174	r=.131 p=.685	
Trunk Fat (%)	r=1 p=----	r=-.291 p=.158	r=-.201 p=.335	r=-.372 p=.17	r=-.018 p=.957		
Mito Max Oxphos	r=1 p=----	r=.854 p<.001	r=.958 p<.001	r=.821 p=.001			
Mito Max ETS	r=1 p=----	r=.829 p<.001	r=.771 p=.003				
Mito C1 Resp.	r=1 p=----	r=.773 p=.003					

Table S4. Pearson Bivariate correlation matrix depicting the interrelationships between measures of adiposity (BMI, whole-body fat %, trunk fat %) and mitochondrial respiratory function. R-value and p-value of the correlation is listed. Note the lack of correlation between adiposity and BMI and measures of mitochondrial function in this population.

Table S5

Model 1: Predicting Mitochondrial Max Oxidative Capacity [(ρmol/(s*mg)]

	β coefficient					
	β	**Std. Error**	**t**	**Sig.**	**β 95% CI**	**Partial Eta Squared**
Model				<.001		
Intercept	49.7	17.1	2.9	.009	(14 – 85.4)	2.9
Whole-body fat (%)	.081	.414	.196	.847	(-.8 - .94)	.002
CKD Stage 1&2	40.12	6.4	6.3	<.001	(26.8-53.4)	.664
CKD Stage 3	18.02	7.1	2.6	.02	(3.2-32.8)	.243
CKD Stage 4&5	Reference Stage					

Mode R^2 = .68

Model 2: Predicting Mitochondrial Max Oxidative Capacity [(ρmol/(s*mg)]

	β coefficient					
	β	**Std. Error**	**t**	**Sig.**	**β 95% CI**	**Partial Eta Squared**
Model				<.001		
Intercept	63.02	17.8	3.5	.002	(25.9 – 100.1)	.374
BMI	-.261	.452	-.578	.57	(-1.2 - .68)	.016
CKD Stage 1&2	40.9	6.24	6.6	<.001	(27.9 - 53.9)	.672
CKD Stage 3	15.28	6.9	2.24	.036	(1.1 – 29.9)	.193
CKD Stage 4&5	Reference Stage					

Mode R^2 = .703

Table S5. Linear regression model to determine mitochondrial function (max oxidative respiration capacity - [(ρmol/(s*mg)]). Score from CKD stage, and body fat percentage (model 1), and BMI (model 2). Beta coefficients for each predictor represent change in mitochondrial oxidative capacity due to CKD stage (Stage 1&2, Stage 3, in reference to Stage 4&5) or 1 unit change in body fat percentage (model 1) or BMI (model 2). Model significance, amount of variance in mitochondrial oxidative capacity explained by the model (R^2), is shown in the bottom panel. Partial eta squared represents the effect size of each predictor.

Table S6

	14 Subjects (without enzyme analysis)	13 Subjects (with enzyme analysis)	P-Value
Age	59.6 (9.9)	59.3 (6.3)	.69 (ns)
Years of DM	16 (7)	13.8 (7.1)	.99 (ns)
HbA1c (%)	7.6 (5.6)	8 (6.8)	.89 (ns)
Whole body lean mass (kg)	56.6 (10.1)	58.2 (12.8)	.48 (ns)
OGTT (AUC)	43514 (11372)	41782 (12274)	.7 (ns)
BMI (kg/m^2)	34.8 (5.6)	35.9 (6.8)	.73 (ns)
eGFR	46.2 (35.2)	57.14 (26.3)	.36 (ns)
Mito LEAK	5.7 (2.5)	5.62 (1.85)	.24 (ns)
Mito C1 Respiration	45.2 (13.6)	35.5 (13.5)	.68 (ns)
Mito max OxPhos	79.9 (20.8)	64.4 (20.3)	.93 (ns)
Mito max ETS	89.9 (18.4)	99.5 (27.6)	.114 (ns)
PPT Score	22.7 (8.3)	27.5 (6.8)	.56 (ns)
Knee Extensor Torque	41.4 (30.2)	55.4 (31)	.78 (ns)
Hip Extensor Torque	90.6 (47.1)	110 (48.0)	.53 (ns)
Knee Extensor Power	64.8 (60.4)	106 (58)	.87 (ns)

Table S6. Independent samples t-test to assess whether there are differences between those with muscle samples undergoing mitochondrial enzymatic testing (13 participants), and those that did not have muscle samples enzymatically tested (n=14). Neither group differed in any major outcome measure (independent samples t-test, α = .05).

Supplemental Figures

FIG S1

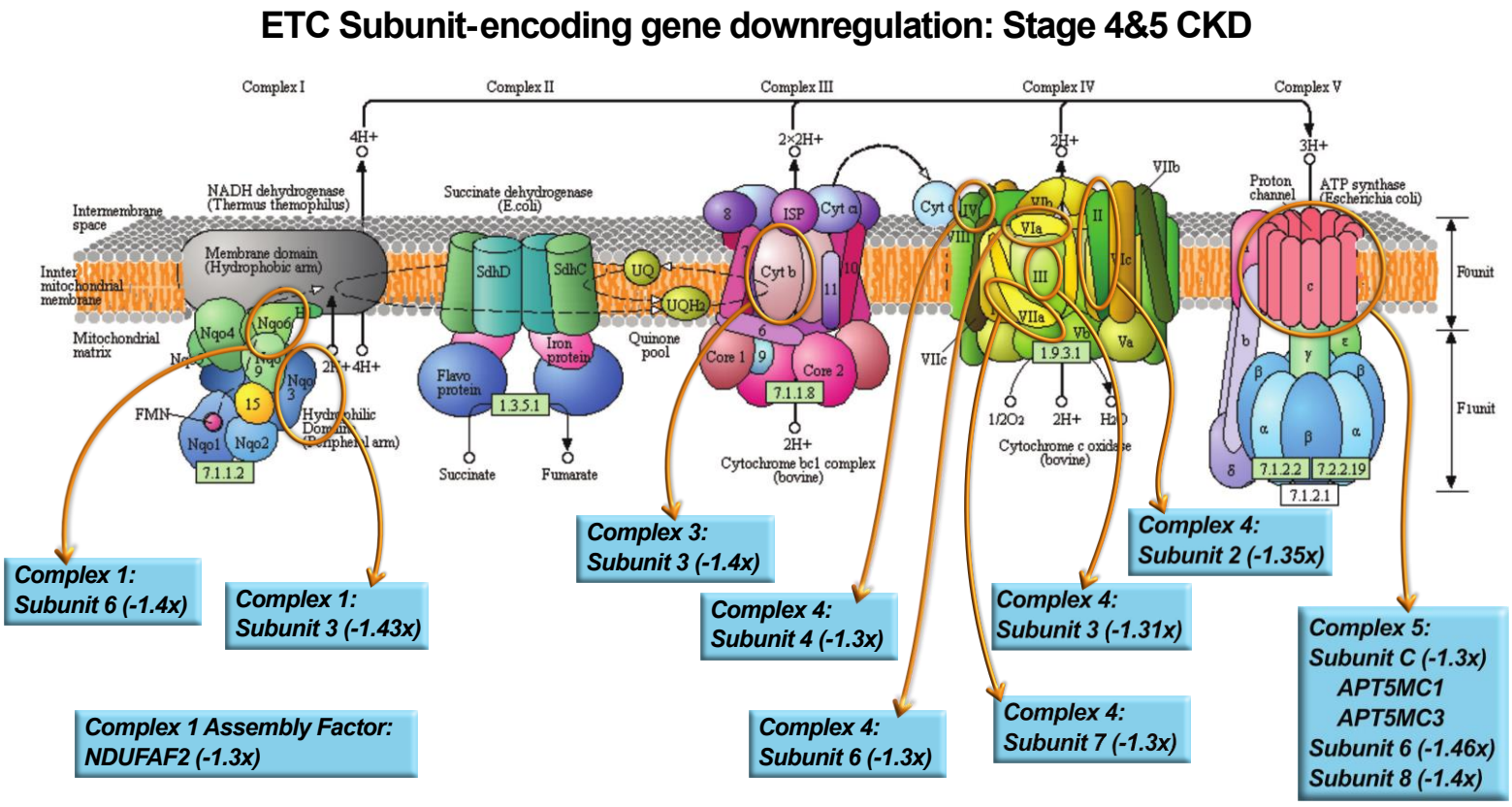

Figure S1. ETC Subunit Gene Expression

KEGG oxidative phosphorylation pathway annotation for stage 4&5 CKD muscle. Significant selected downregulated genes in the electron transport chain GO term were used to annotate the mitochondrial electron transport chain subunits they encode (subunits circled in yellow, and connected to their corresponding gene with black arrow, and highlighted in blue). Not pictured – NDUFAF2 (complex 1 assembly factor) and SURF1 (complex 4 assembly factor). All listed genes are significantly downregulated in late-stage (4&5) CKD compared to early (stage 1&2).

FIG S2.

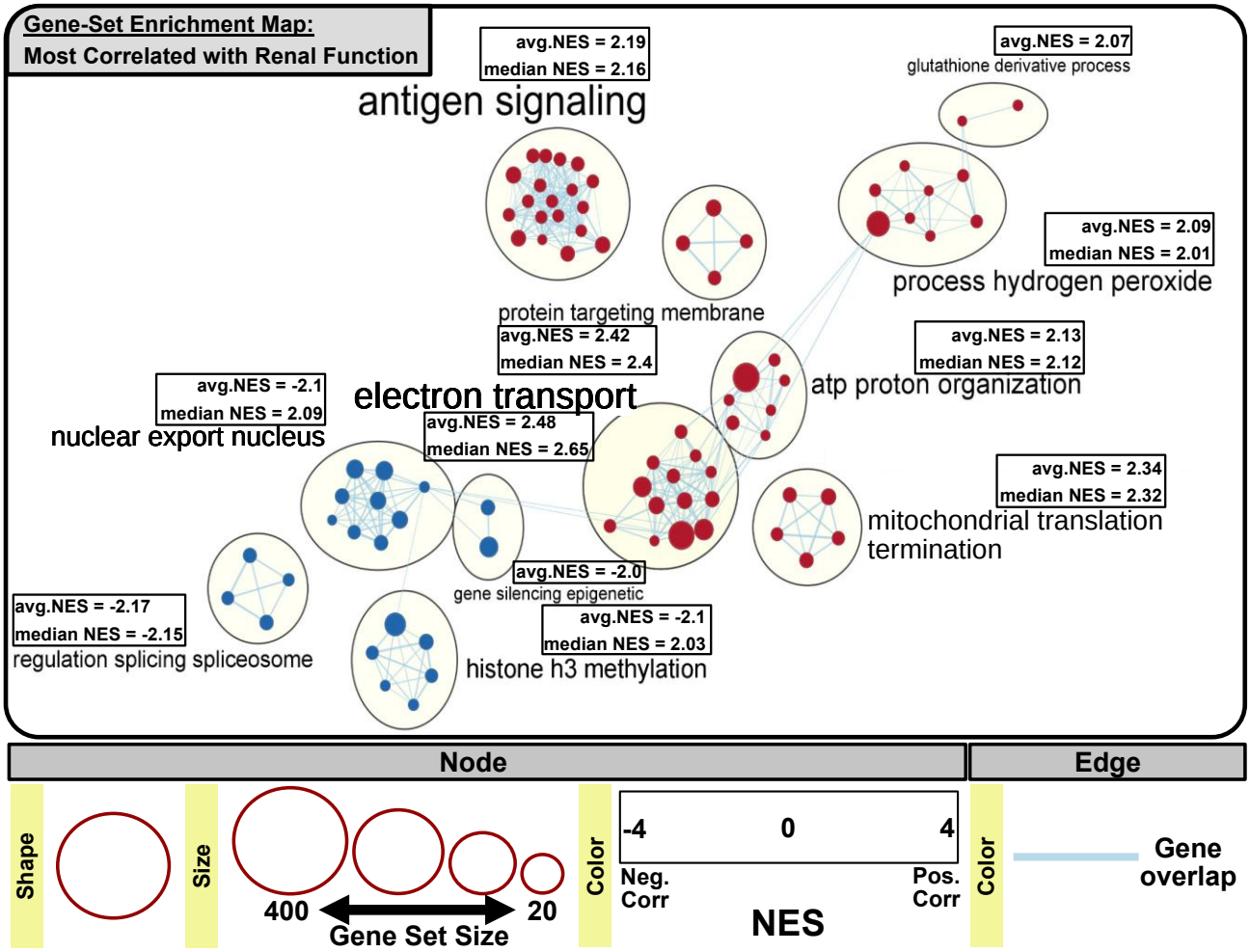

Figure S2. Gene Set Enrichment Map

Gene Set Enrichment Map of transcriptional pathways most strongly correlated to renal function (eGFR), either positively correlated (red) or negatively correlated (blue). Biological pathways are ranked and scored by net enrichment (NES) ranging from -4 (transcriptional pathways enriched in the negatively correlated grouping) to +4 (transcriptional pathways enriched in the positively correlated grouping). Note the clustering of electron transport and its shared pathway – atp proton organization. Eelectron transport represents the gene set most strongly enriched/related to renal function (avg. NES = 2.48).

FIG S3

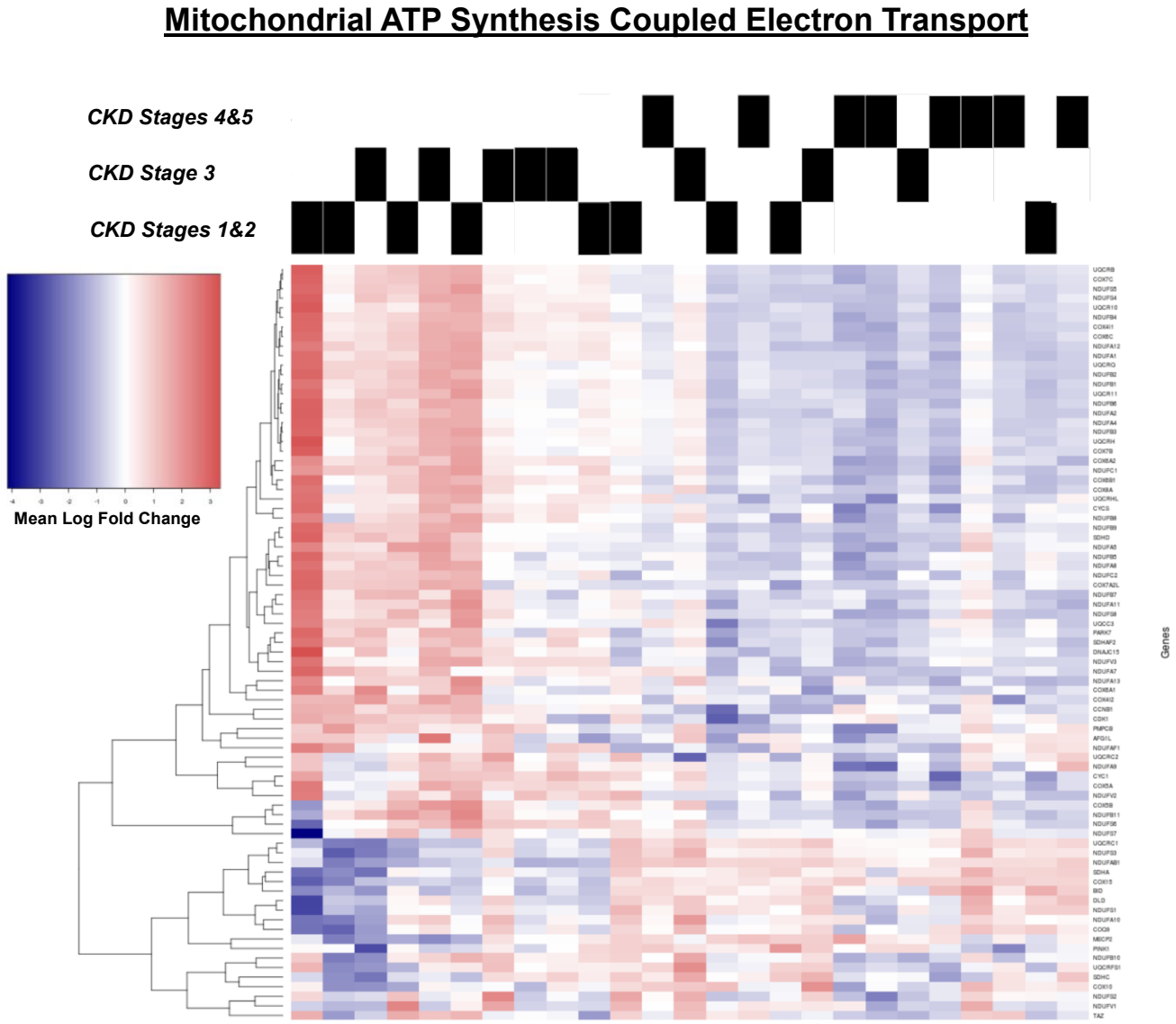

Figure S3. ATP-Synthesis-Coupled Electron Transport Gene Expression Heatmap
GO Biological Function pathway annotation for the Coupled Electron Transport Gene Network across stages of CKD. Colored blocks indicate significant differentially expressed genes with the ATP-coupled electron transport network (color code shown in the inlayed key – red = upregulation, blue = downregulation, expressed in mean log fold change from -4 to 4). Note the clustering of early-stage CKD participants exhibiting upregulation of coupled ATP synthesis genes, with gradual reduction in expression, generally, upon CKD stage progression.

FIG.S4

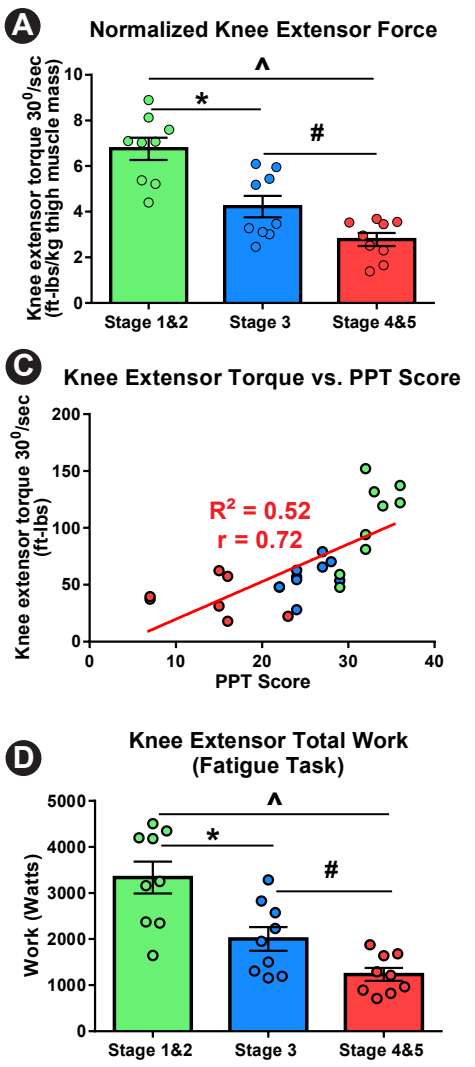

B

	PPT Score	Hip Extensor Torque (30⁰/sec)	Knee Extensor Torque (30⁰/sec)	Knee Extensor Work (fatigue)	Chair Rise Score	50-ft walk time
PPT Score	r=1 p=----	r=.88 p<.001	r=.78 p<.001	r=.74 p<.001	r=.87 p<.001	r=-.954 p<.001
Hip Extensor Torque (30⁰/sec)		r=1 p=----	r=.898 p<.001	r=.823 p<.001	r=.723 p<.001	r=-.608 p<.001
Knee Extensor Torque (30⁰/sec)			r=1 p=----	r=.904 p<.001	r=.784 p<.001	r=-.747 p<.001
Knee Extensor Work (fatigue)				r=1 p=----	r=.769 p<.001	r=-.654 p<.001
Chair Rise Score					r=-.697 p<.001	r=.821 p<.001
50-ft walk time						r=1 p=----

Figure S4. Muscle Performance and Physical Function Interrelationships

A. Knee extensor torque production was normalized to thigh region lean mass (as assessed by DXA) to obtain knee extensor force production per unit muscle volume, and compared across stages of CKD progression via 1-way ANOVA. Bar heights represent group mean and error bars represent + SEM. (F=22..21, p<.001). **B**. Pearson Bivariate Correlation matrix between measures of physical function capacity (PPT score, chair rise score, 50-ft. walk time/gait speed) and muscle performance metrics (knee and hip extensor force production and knee extensor fatigue resistance – denoted as total work performed by the knee extensors over the fatigue task). **C.** Pearson Bivariate Correlation plot demonstrating the strong correlation between knee extensor torque and PPT score. Dots indicate individual pariticipant – red (stage 4&5 CKD), blue (stage 3 CKD), green (stage 1&2). **D.** Knee extensor total work over the fatigue task was compared across stages of CKD progression via 1-way ANOVA. Bar heights represent group mean and error bars represent + SEM. (F=16.4, p<.001). The following symbols represent significant post-hoc tests of pairwise comparisons (tukey post-hoc): *(between Stage 1&2 and Stage 3), ^(between stage 1&2 and Stage 4&5), #(Between stage 3 and Stage 4&5) (all p<.05).

FIG. S5

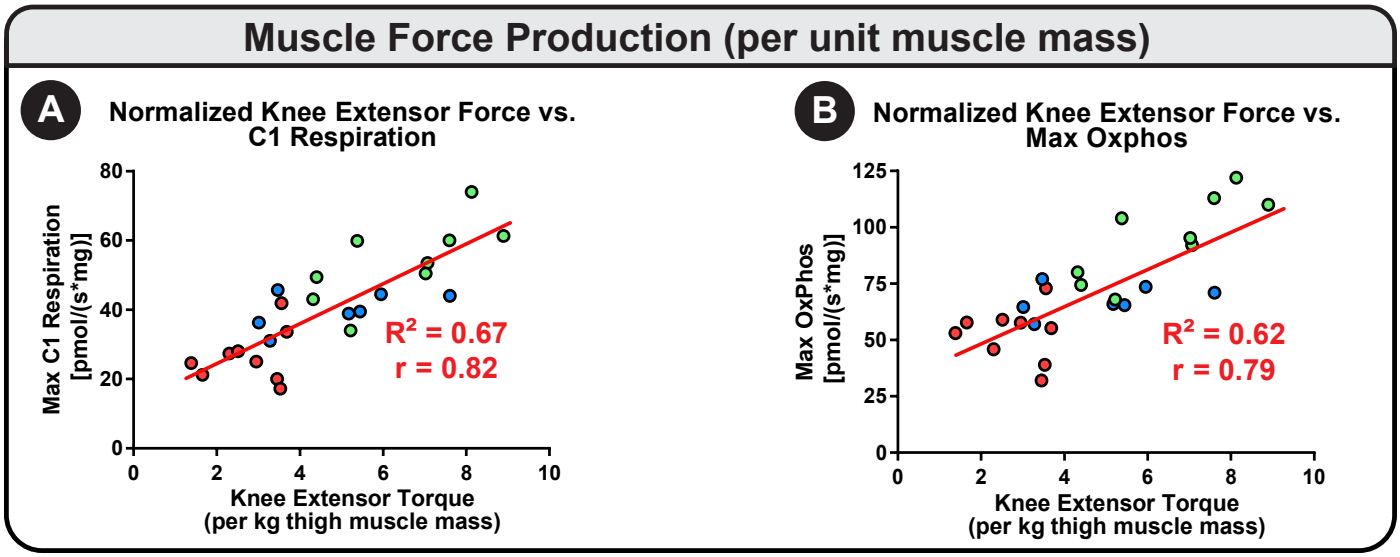

Figure S5. Mitochondrial function and ATP-production capacity relates to contractile force per unit muscle volume

A. Pearson Bivariate Correlation, in which knee extensor torque production was normalized to thigh region lean mass (as assessed by DXA) to obtain knee extensor force production per unit muscle volume, and correlated to mitochondrial respiration through complex 1 (r^2=.67, p<.001). **B**. Pearson Bivariate Correlation matrix between normalized knee extensor force production and maximal mitochondrial oxidative capacity (r^2=.62, p<.001).

FIG. S6

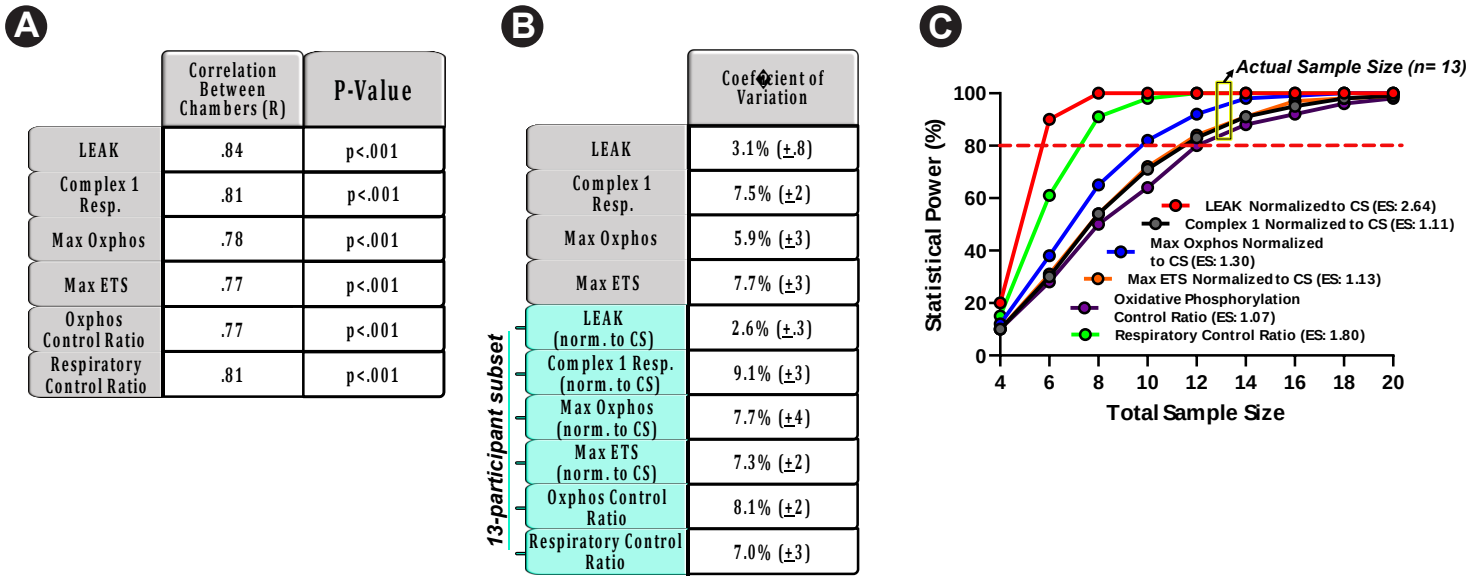

	Correlation Between Chambers (R)	P-Value
LEAK	.84	p<.001
Complex 1 Resp.	.81	p<.001
Max Oxphos	.78	p<.001
Max ETS	.77	p<.001
Oxphos Control Ratio	.77	p<.001
Respiratory Control Ratio	.81	p<.001

	Coefficient of Variation
LEAK	3.1% (±.8)
Complex 1 Resp.	7.5% (±2)
Max Oxphos	5.9% (±3)
Max ETS	7.7% (±3)
LEAK (norm. to CS)	2.6% (±.3)
Complex 1 Resp. (norm. to CS)	9.1% (±3)
Max Oxphos (norm. to CS)	7.7% (±4)
Max ETS (norm. to CS)	7.3% (±2)
Oxphos Control Ratio	8.1% (±2)
Respiratory Control Ratio	7.0% (±3)

13-participant subset

Figure S6. Mitochondrial Respiration Measurement Variability and effects of normalization.

A. Pearson Bivariate Correlations were performed between prepared muscle bundles from the same biopsy in each of the 2 Oroborous oxygraphy chambers. Correlations were assessed for each major respiration output measure in each muscle sample pair from each participant. **B.** Coefficient of Variation (CV) was assessed for duplicate respiration measures for each respiration output for each participant using the root mean square method as previously described (**S39**). The highlighted portion of the table indicates CV calculated for the 13-participant subset that possessed CS enzyme activity measures used for normalization for these samples (CKD stage 1&2- n=5, CKD Stage 3 – n=5, CKD Stage 4&5 – n=3, shown in Table 2) (error bars represent SD). **C.** Statistical Power Plot of the CS-normalized respiration measures depicted in table 2 of the manuscript. Effect sizes were all moderate-strong (ES ranging from 1.07-2.64), and when setting the α (type 1 error rate) are 5%, and β (type 2 error rate) at 20%, we find that we were adequately powered to detect significant differences in these respiration measures (our sample size of n=13 eclipsed the 80% power threshold for all CS-normalized measures).

Supplemental References

S1. Brown M, Sinacore DR, Binder EF, et al. Physical and performance measures for the identification of mild to moderate frailty. J Gerontol A Biol Sci Med Sci. Jun 2000;55(6):M350-355.

S2. Reuben DB, Siu AL. An objective measure of physical function of elderly outpatients. The Physical Performance Test. J Am Geriatr Soc. Oct 1990;38(10):1105-1112.

S3. Reuben DB, Siu AL, Kimpau S. The predictive validity of self-report and performance-based measures of function and health. J Gerontol. Jul 1992;47(4):M106-110.

S4. Worrell TW, Karst G, Adamczyk D, et al. Influence of joint position on electromyographic and torque generation during maximal voluntary isometric contractions of the hamstrings and gluteus maximus muscles. J Orthop Sports Phys Ther. Dec 2001;31(12):730-740.

S5. Frey-Law LA, Laake A, Avin KG, et al. Knee and elbow 3D strength surfaces: peak torque-angle-velocity relationships. J Appl Biomech. Dec 2012;28(6):726-737.

S6. Shanely, R.A., Zwetsloot, K.A., Triplett, N.T., et al. (2014) Human skeletal muscle biopsy procedures using the modified bergstrom technique. *J Vis Exp*, (91): 51812

S7. Gonzalez-Freire M, Scalzo P, D'Agostino J, et al. Skeletal muscle ex vivo mitochondrial respiration parallels decline in vivo oxidative capacity, cardiorespiratory fitness, and muscle strength: The Baltimore Longitudinal Study of Aging. Aging Cell. Apr 2018;17(2).

S8. Pesta D, Gnaiger E. High-resolution respirometry: OXPHOS protocols for human cells and permeabilized fibers from small biopsies of human muscle. Methods Mol Biol. 2012;810:25-58.

S9. Leek, B.T., Mudaliar, S.R., Henry, R. et al. (2001) Effect of acute exercise on citrate synthase activity in untrained and trained human skeletal muscle. *Am J Physiol Regul Integr Comp Physiol*, 280(2): R441-7.

S10. Chi MM, Hintz CS, Coyle EF, et al. Effects of detraining on enzymes of energy metabolism in individual human muscle fibers. Am J Physiol. Mar 1983;244(3):C276-287.

S11. McCarthy DJ, Chen Y, Smyth GK. Differential expression analysis of multifactor RNA-Seq experiments with respect to biological variation. Nucleic Acids Res. May 2012;40(10):4288-4297.

S12. Dobin, A., Davis, C.A., Schlesinger, F., et al. (2013) STAR: ultrafast universal RNA-seq aligner. *Bioinformatics*, 29(1): 15-21.

S13. Wang, L., Wang, S., & Li, W. (2012) RSeQC: quality control of rna-seq experiments. *Bioinformatics*, 28(16): 2184-5.

S14. Robinson MD, McCarthy DJ, Smyth GK. edgeR: a Bioconductor package for differential expression analysis of digital gene expression data. Bioinformatics. Jan 1 2010;26(1):139-140.

S15. Luo W, Friedman MS, Shedden K, et al. GAGE: generally applicable gene set enrichment for pathway analysis. BMC Bioinformatics. May 27 2009;10:161.

S16. Luo W, Brouwer C. Pathview: an R/Bioconductor package for pathway-based data integration and visualization. Bioinformatics. Jul 15 2013;29(14):1830-1831.

S17. Subramanian, A., Tamayo, P., Mootha, V.K., Mukherjee, S., Ebert, B.L., Gillette, M.A., et al. (2005) Gene set enrichment analysis: a knowledge-based approch for interpreting genome-wide expression profiles. *PNAS*, 102(43): 15545-15550.

S18. Morin D, Musman J, Pons S, et al. Mitochondrial translocator protein (TSPO): From physiology to cardioprotection. Biochem Pharmacol. Apr 1 2016;105:1-13.

S19. Liu, Y., & Sweeney, G. (2014) Adiponectin action in skeletal muscle. *Best Pract Res Clin Endocrinol Metab*, 28(1): 33-41.

S20. Minokoshi, Y., Toda, C., & Okamoto, S. (2012). Regulatory role of leptin in glucose and lipid metabolism in skeletal muscle. *Indian Journal of Endocrinology and Metabolism*, *16*(Suppl 3), S562–S568.

S21. Miljkovic, I., Kuipers, A., Kuller, L., et al. (2013). Skeletal Muscle Adiposity is associated with Serum Lipid and Lipoprotein Levels in Afro-Caribbean Men. *Obesity (Silver Spring, Md.)*, *21*(9), 1900–1907

S22. Morita, M., & Imanaka, T. (2012) Peroxisomal ABC transporters: structure, function and role in disease. *Biochimica et Biophysica Acta*, 1822(9): 1287-1396.

S23. Wang Z, Cotney J, Shadel GS. Human mitochondrial ribosomal protein MRPL12 interacts directly with mitochondrial RNA polymerase to modulate mitochondrial gene expression. J Biol Chem. Apr 27 2007;282(17):12610-12618.

S24. Uittenbogaard, M., Brantner, C.A., & Chiaramello, A. (2018) Epigenetic modifiers promote mitochondrial biogenesis and oxidative metabolism leading to enhanced differentiation of neuroprogenitor cells. *Cell Death & Disease*, 9: 360.

S25. Kravic, B., Harbauer, A.B., Romanello, V., et al. (2018) In mammalian skeletal muscle, phosphorylation of TOMM22 by protein kinase CSNK2/CK2 controls mitophagy. *Autophagy*, 14(2): 311-335.

S26. Srivastava, S., Savanur, M.A., Sinha, D., Birje, A., Vigneshwaran, R., Saha, P., & D'Silva, P. (2017) Regulation of mitochondrial protein import by the nucleotide exchange factors GrpEL1 and GrpEL2 in human cells. *J Biol Chem*, 292(44): 18075-18090.

S27. Fiedorczuk, K., & Sazanov, L.A. (2018) Mammalian mitochondrial complex 1 structure and disease-causing mutations. *Trends Cell Biol*, 28(10): 835-867.

S28. Tsujimoto, Y., & Shimizu, S. (2000) VDAC regulation by the Bcl-2 family of proteins. *Cell Death & Differentiation*, 7(12): 1174-81.

S29. Hu, C., Huang, Y., & Li, L. (2017) Drp1-dependent mitochondrial fission plays critical roles in physiological and pathological progresses in mammals. *Int J Mol Sci*, 18(1): 144.

S30. Marquez, R.T., & Xu, L. (2012) Bcl-2:beclin 1 complex: multiple, mechanisms regulating autophagy/apoptosis toggle switch. *Am J Cencer Res*, 2(2): 214-221.
S31. Gal, A., Balicza, P., Weaver, D., Naghdi, S., Joseph, S.K., Varnai, P., Gyuris, T., et al. (2017) MSTO1 is a cytoplasmic pro-mitochondrial fusion protein, whose mutation induces myopathy and ataxia in humans. *EMBO Mol Med*, 9(7): 967-984.
S32. Ellisen LW, Ramsayer KD, Johannessen CM, et al. REDD1, a developmentally regulated transcriptional target of p63 and p53, links p63 to regulation of reactive oxygen species. Mol Cell. Nov 2002;10(5):995-1005.
S33. Geng, J., Wei, M., Yuan, X., et al (2019) TIGAR regulates mitochondrial functions through sirt1-pgc1α pathway and translocation of tiger into mitochondria in skeletal muscle. *FASEB J*, 33(5): 6082-6098.
S34. Matta, S., Pareek, G., Bankapalli, K., Oblesha, A., & D'Silva, P. (2017) Role of tim17 transmembrane regions in regulating the architecture of presequence translocase and mitochondrial dna stability. *Mol Cell Biol*, 37(6): e00491-16.
S35. Murphy, M.P. (2019) Rerouting metabolism to activate macrophages. *Nat Immunol*, 20(9): 1097-1099.
S36. Jang, D. G., Sim, H. J., Song, E. K., et al (2015). A thioredoxin fold protein Sh3bgr regulates Enah and is necessary for proper sarcomere formation. *Developmental Biology*, *405*(1), 1–9.
S37. Li, Y., Li, J., Zhu, J., et al. (2007) Decorin gene transfer promotes muscle cell differentiation and muscle regeneration. *Mol Ther*, 15(9): 1616-22.
S38. Braczynski AK, Vlaho S, Muller K, et al. ATP synthase deficiency due to TMEM70 mutation leads to ultrastructural mitochondrial degeneration and is amenable to treatment. Biomed Res Int. 2015;2015:462592.
S39. Hyslop, N.P., & White, W.H. (2009) Estimating prevision using duplicate measurements. Journal of the Air and Waste Manamgement Association. 59: 1032-1039.